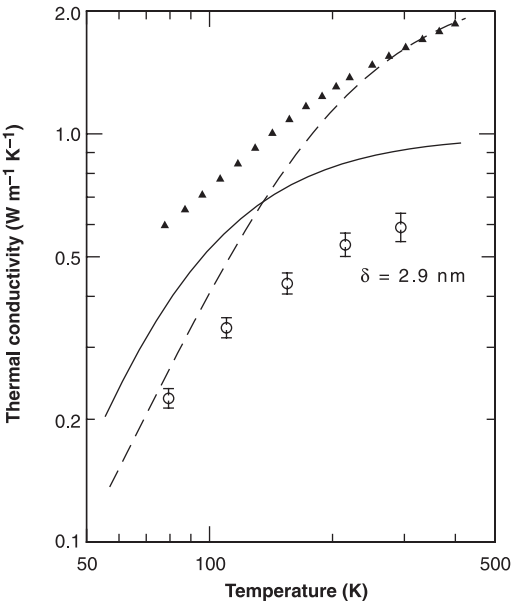

Fig. 2. Temperature dependence of the thermal conductivity of the W/Al_2O_3 nanolaminate deposited at 177°C when $\delta = 2.9$ nm (open circles). Data for a fully dense amorphous Al_2O_3 film prepared by ion-beam sputtering (solid triangles) (*7*) are included for comparison. The dashed line is the calculated minimum conductivity Λ_{min} for alumina; the solid line is $\Lambda = \delta G_{DMM}$, where $\delta = 2.9$ nm and G_{DMM} is the calculated conductance of W/Al_2O_3 interfaces under the diffuse mismatch model (*19*).

expected thermal conductivity, assuming a constant $G = 260$ MW m^{-2} K^{-1} and fixed values for the thermal conductivities of the individual alumina and W layers. For the ALD nanolaminate with $1/\delta = 0.35$ nm^{-1} and a deposition temperature of 177°C, the thermal conductivity was almost wholly dominated by this interface conductance, i.e., $\Lambda \approx \delta G$.

This experimental value for G is close to the prediction of the diffuse mismatch model (DMM) (*19*). In this model of interface thermal transport, lattice vibrations are assumed to be scattered strongly at the interface and to have a transmission coefficient given by the ratio of the densities of vibrational states on either side of the interface. Using a Debye model for the densities of states, we calculated that $G_{DMM} = 320$ MW m^{-2} K^{-1} for W/Al_2O_3. Typically, the DMM overestimates the conductance near room temperature, because this model, when based on a Debye density of states, does not take into account the dispersion of the vibrational modes.

We continued the comparison between our data and the G_{DMM} by examining the temperature dependence of the thermal conductivity (Fig. 2). The solid line in Fig. 2 is $\Lambda = \delta G_{DMM}$; that is, the solid line shows the thermal conductivity of a hypothetical nanolaminate in which δ is 2.9 nm and the thermal conductivity is dominated by the diffuse mismatch value of the thermal conductance of the W/Al_2O_3 interfaces. The temperature dependence of the data and G_{DMM} are similar, giving further support to our assertion that thermal transport in the nanolaminates is mostly controlled by the conductance of the interfaces.

Interfaces between dissimilar materials such as W and Al_2O_3 are effective in reducing the thermal conductivity of nanostructured materials, but the relatively high interface energy will limit the stability of these materials at the high service temperatures typically required of thermal barrier coatings. Applications of nanolaminates as thermal barriers at temperatures higher than 1000°C would require the development of material interfaces that satisfy the conflicting demands of low thermal conductance and exceptional thermal stability.

References and Notes

1. D. G. Cahill *et al.*, *J. Appl. Phys.* **93**, 793 (2003).
2. N. P. Padture, M. Gell, E. H. Jordan, *Science* **296**, 280 (2002).
3. S. T. Huxtable *et al.*, *Appl. Phys. Lett.* **80**, 1737 (2002).
4. K. E. Goodson, *J. Heat Transfer* **118**, 279 (1996).
5. C.-W. Nan, R. Birringer, D. R. Clarke, H. Gleiter, *J. Appl. Phys.* **81**, 6692 (1997).
6. R. J. Stoner, H. J. Maris, *Phys. Rev. B* **48**, 16373 (1993).
7. S.-M. Lee, D. G. Cahill, T. H. Allen, *Phys. Rev. B* **52**, 253 (1995).
8. D. P. H. Hasselman *et al.*, *Am. Ceram. Soc. Bull.* **66**, 799 (1987).
9. K. W. Schlichting, N. P. Padture, P. G. Klemens, *J. Mater. Sci.* **36**, 3003 (2001).
10. G. Soyez *et al.*, *Appl. Phys. Lett.* **77**, 1155 (2000).
11. Materials and methods are available as supporting material on *Science* Online.
12. A. C. Dillon, A. W. Ott, J. D. Way, S. M. George, *Surf. Sci.* **322**, 230 (1995).
13. J. W. Klaus, S. J. Ferro, S. M. George, *Thin Solid Films* **360**, 145 (2000).
14. C. A. Paddock, G. L. Eesley, *J. Appl. Phys.* **60**, 285 (1986).
15. D. A. Young, C. Thomsen, H. T. Grahn, H. J. Maris, J. Tauc, in *Phonon Scattering in Condensed Matter*, A. C. Anderson, J. P. Wolfe, Eds. (Springer, Berlin, 1986), p. 49–51.
16. D. G. Cahill, K. E. Goodson, A. Majumdar, *J. Heat Transfer* **124**, 223 (2002).
17. R. M. Costescu, M. A. Wall, D. G. Cahill, *Phys. Rev. B* **67**, 54302 (2003).
18. A. Feldman, *High Temp. High Pressures* **31**, 293 (1999).
19. E. T. Swartz, R. O. Pohl, *Rev. Mod. Phys.* **61**, 605 (1989).

20. Supported by NSF grant no. CTS-0319235, U.S. Department of Energy (DOE) grant no. DEFG02-01-ER45938, and the Air Force Office of Scientific Research. Sample characterization used the Laser Facility of the Seitz Materials Research Laboratory and the facilities of the Center for Microanalysis of Materials, which is partially supported by DOE under grant no. DEFG02-91-ER45439.

Supporting Online Material

sciencemag.org/cgi/content/full/303/5660/989/DC1
Materials and Methods
References and Notes

17 November 2003; accepted 29 December 2003

Improving the Density of Jammed Disordered Packings Using Ellipsoids

Aleksandar Donev,[1,4] Ibrahim Cisse,[2,5] David Sachs,[2] Evan A. Variano,[2,6] Frank H. Stillinger,[3] Robert Connelly,[7] Salvatore Torquato,[1,3,4]* P. M. Chaikin[2,4]

Packing problems, such as how densely objects can fill a volume, are among the most ancient and persistent problems in mathematics and science. For equal spheres, it has only recently been proved that the face-centered cubic lattice has the highest possible packing fraction $\varphi = \pi/\sqrt{18} \approx 0.74$. It is also well known that certain random (amorphous) jammed packings have $\varphi \approx 0.64$. Here, we show experimentally and with a new simulation algorithm that ellipsoids can randomly pack more densely—up to $\varphi = 0.68$ to 0.71 for spheroids with an aspect ratio close to that of M&M's Candies—and even approach $\varphi \approx 0.74$ for ellipsoids with other aspect ratios. We suggest that the higher density is directly related to the higher number of degrees of freedom per particle and thus the larger number of particle contacts required to mechanically stabilize the packing. We measured the number of contacts per particle $Z \approx 10$ for our spheroids, as compared to $Z \approx 6$ for spheres. Our results have implications for a broad range of scientific disciplines, including the properties of granular media and ceramics, glass formation, and discrete geometry.

The structure of liquids, crystals, and glasses is intimately related to volume fractions of ordered and disordered (random) hard-sphere packings, as are the transitions between these phases (*1*). Packing problems (*2*) are of current interest in dimensions higher than three

for insulating stored data from noise (*3*), and in two and three dimensions in relation to flow and jamming of granular materials (*4*–*6*) and glasses (*7*). Of particular interest is random packing, which relates to the ancient (economically important) problem of how much grain a barrel can hold.

Many experimental and computational algorithms produce a relatively robust packing fraction (relative density) $\varphi \approx 0.64$ for randomly packed monodisperse spheres as they proceed to their limiting density (*8*). This number, widely designated as the random close packing (RCP) density, is not universal but generally depends on the packing protocol (*9*). RCP is an ill-defined concept because higher packing fractions are obtained as the system becomes ordered, and a definition for randomness has been lacking. A more recent concept is that of the maximally random jammed (MRJ) state, corresponding to the least ordered among all jammed packings (*9*). For a variety of order metrics, it appears that the MRJ state has a density of $\varphi \approx 0.637$ and is consistent with what has traditionally been thought of as RCP (*10*). Henceforth, we refer to this random form of packing as the MRJ state.

We report on the density of the MRJ state of ellipsoid packings as asphericity is introduced. For both oblate and prolate spheroids, φ and Z (the average number of touching neighbors per particle) increase rapidly, in a cusp-like manner, as the particles deviate from perfect spheres. Both reach high densities such as $\varphi \approx 0.71$, and general ellipsoids pack randomly to a remarkable $\varphi \approx 0.735$, approaching the density of the crystal with the highest possible density for spheres (*11*) $\varphi = \pi/\sqrt{18} \approx 0.7405$. The rapid increases are unrelated to any observable increase in order in these systems that develop neither crystalline (periodic) nor liquid crystalline (nematic or orientational) order.

Our experiments used two varieties of M&M's Milk Chocolate Candies: regular and baking ("mini") candies (*12*). Both are oblate spheroids with small deviations from true ellipsoids, $\Delta r/r < 0.01$. Additionally, M&M's Candies have a very low degree of polydispersity (principal axes $2a = 1.34 \pm 0.02$ cm, $2b = 0.693 \pm 0.018$ cm, $a/b = 1.93 \pm 0.05$ for regular; $2a = 0.925 \pm 0.011$ cm, $2b = 0.493 \pm 0.018$ cm, $a/b = 1.88 \pm 0.06$ for minis). Several sets of experiments were performed to determine the packing fraction. A square box, 8.8 cm by 8.8 cm, was filled to a height of 2.5 cm while shaking and tapping the container. The actual measurements were performed by adding 9.0 cm to the height and excluding the contribution from the possibly layered bottom. After measuring the average mass, density, and volume of the individual candies, the number of candies in the container and their volume fraction could be simply determined by weighing. These experiments yielded $\varphi = 0.665 \pm 0.01$ for regulars and $\varphi = 0.695 \pm 0.01$ for minis. The same technique was used for 3.175 = mm ball bearings (spheres) and yielded $\varphi = 0.625 \pm 0.01$. A second set of experiments was performed by filling 0.5-, 1-, and 5-liter round flasks (to minimize ordering due to wall effects) with candies by pouring them into the flasks while tapping (5 liters corresponds to about 23,000 minis or 7500 regulars) (Fig. 1A). The volume fractions found in these more reliable studies were $\varphi = 0.685 \pm 0.01$ for both the minis and regulars (*13*). The same procedure for 30,000 ball bearings in the 0.5-liter flask yielded $\varphi = 0.635 \pm 0.01$, which is close to the accepted MRJ density.

A 5-liter sample of regular candies similar to that shown in Fig. 1A was scanned in a medical magnetic resonance imaging device at Princeton Hospital. For several planar slices, the direction θ (with respect to an arbitrary axis) of the major elliptical axis was manually measured and the two-dimensional nematic order parameter $S_2 = \langle 2\cos^2\theta - 1 \rangle$ was computed, yielding $S_2 \approx 0.05$. This is consistent with the absence of orientational order in the packing (*14*).

Our simulation technique generalizes the Lubachevsky-Stillinger (LS) sphere-packing algorithm (*15*, *16*) to the case of ellipsoids. The method is a hard-particle molecular dynamics (MD) algorithm for producing dense disordered packings. Initially, small ellipsoids are randomly distributed and randomly oriented in a box with periodic boundary conditions and without any overlap. The ellipsoids are given velocities and their motion followed as they collide elastically and also expand uniformly. After some time a jammed state with a diverging collision rate is reached and the density reaches a maximal value. A novel event-driven MD algorithm (*17*) was used to implement this process efficiently, based on the algorithm used in (*15*) for spheres and similar to the algorithm used for needles in (*18*). A typical configuration of 1000 oblate ellipsoids (aspect ratio $\alpha = b/a = 1.9^{-1} \approx 0.526$) is shown in Fig. 1B, with density of $\varphi \approx 0.70$ and nematic order parameter $S \approx 0.02$ to 0.05.

We have verified that the sphere packings produced by the LS algorithm are jammed according to the rigorous hierarchical definitions of local, collective, and strict jamming (*19*, *20*). Roughly speaking, these definitions are based on mechanical stability conditions that require that there be no feasible local or collective particle displacements and/or boundary deformations. On the basis of our experience with spheres (*10*), we believe that our algorithm (with rapid particle expansion) produces final states that represent the MRJ state well. The algorithm closely reproduces the packing fraction measured experimentally.

The density of simulated packings of 1000 particles is shown in Fig. 2A. Note the two clear maxima with $\varphi \approx 0.71$, already close to the 0.74 for the ordered face-centered cubic (fcc)/hexagonal close-packed (hcp) packing, and the cusp-like minimum near $\alpha = 1$ (spheres). Previous simulations for random sequential addition (RSA) (*21*), as well as gravitational deposition (*22*), produce a similarly shaped curve, with a maximum at nearly the same aspect ratios $\alpha \approx 1.5$ (prolate) or $\alpha \approx 0.67$ (oblate), but with substantially lower volume fractions (such as $\varphi \approx 0.48$ for RSA).

Why does the packing fraction initially increase as we deviate from spheres? The rapid increase in packing fraction is attributable to the expected increase in the number of contacts resulting from the additional rotational degrees

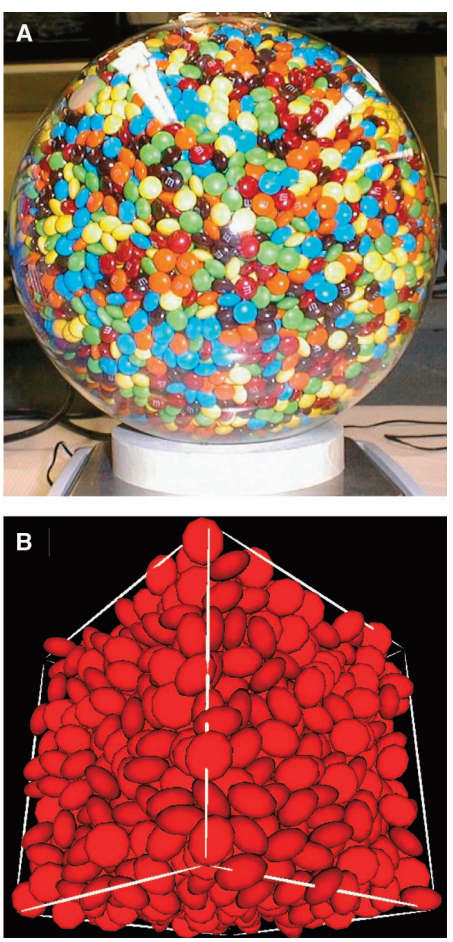

Fig. 1. (**A**) An experimental packing of the regular candies. (**B**) Computer-generated packing of 1000 oblate ellipsoids with $\alpha = 1.9^{-1}$.

[1]Program in Applied and Computational Mathematics, [2]Department of Physics, [3]Department of Chemistry, Princeton University, Princeton, NJ 08544, USA. [4]Princeton Materials Institute, Princeton, NJ 08544, USA. [5]North Carolina Central University, Durham, NC 27707, USA. [6]Department of Civil and Environmental Engineering, [7]Department of Mathematics, Cornell University, Ithaca, NY 14853, USA.

*To whom correspondence should be addressed. E-mail: torquato@princeton.edu

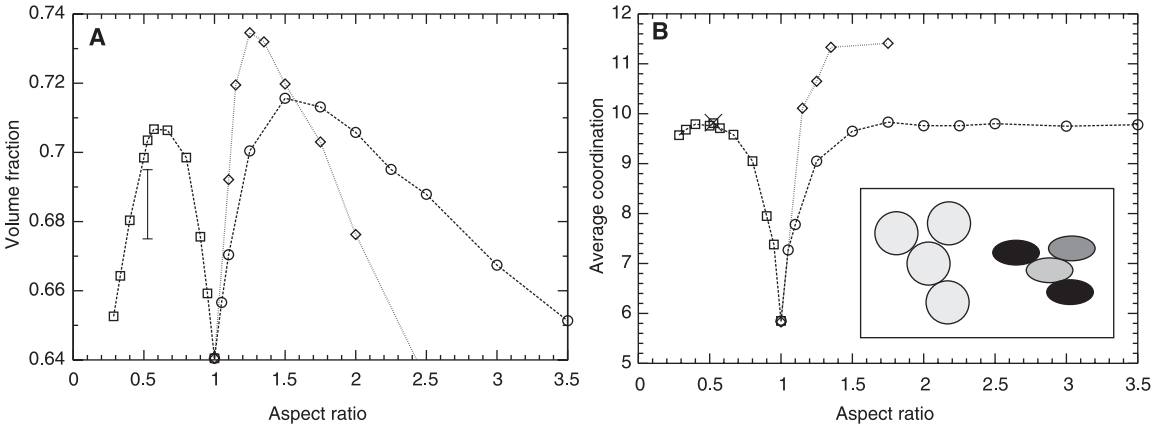

Fig. 2. (**A**) Density φ versus aspect ratio α from simulations, for both prolate (circles) and oblate (squares) ellipsoids as well as fully aspherical (diamonds) ellipsoids. The most reliable experimental result for the regular candies (error bar) is also shown; this likely underpredicts the true density (*38*). (**B**) Mean contact number *Z* versus aspect ratio α from simulations [same symbols as in (A)], along with the experimental result for the regular candies (cross). Inset: Introducing asphericity makes a locally jammed particle free to rotate and escape the cage of neighbors.

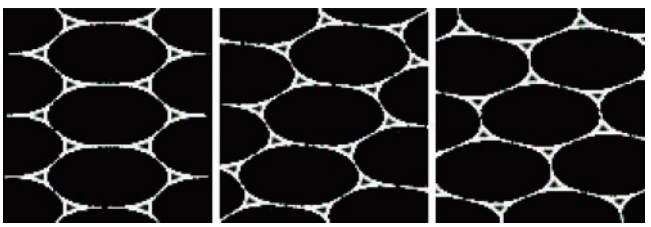

Fig. 3. Shearing the densest packing of ellipses.

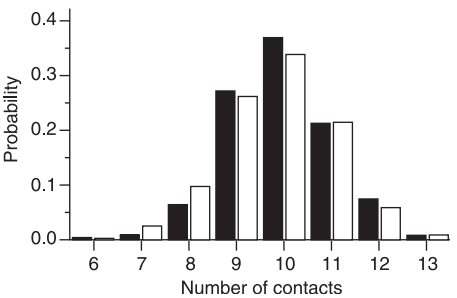

Fig. 4. Comparison of experimental (black bars, from 489 regular candies) and simulated (white bars, from 1000 particles) distribution of particle contact numbers.

of freedom of the ellipsoids. More contacts per particle are needed to eliminate all local and collective degrees of freedom and ensure jamming, and forming more contacts requires a denser packing of the particles. In the inset in Fig. 2B, the central circle is locally jammed. A uniform vertical compression preserves φ, but the central ellipsoid can rotate and free itself and the packing can densify. The decrease in the density for very aspherical particles could be explained by strong exclusion-volume effects in orientationally disordered packings (*23*). Results resembling those shown in Fig. 2A are also obtained for isotropic random packings of spherocylinders (*23*, *24*), but an argument based on "caging" (not jamming) of the particles was given to explain the increase in density as asphericity is introduced. Spherocylinders have a very different behavior for ordered packings from ellipsoids (the conjectured maximal density is $\pi/\sqrt{12} \approx 0.91$, which is significantly higher than for ellipsoids), and also cannot be oblate and are always axisymmetric. The similar positioning of the maximal density peak for different packing algorithms and particle shapes indicates the relevance of a simple geometrical explanation.

By introducing orientational and translational order, it is expected that the density of the packings can be further increased, at least up to 0.74. As shown in Fig. 3 for two dimensions, an affine deformation (stretch) of the densest disk packing produces an ellipse packing with the same volume fraction. However, this packing, although the densest possible, is not strictly jammed (i.e., it is not rigid under shear transformations). The figure shows through a sequence of frames how one can distort this collectively jammed packing (*20*), traversing a whole family of densest configurations. This mechanical instability of the ellipse packing as well as the three-dimensional ellipsoid packing arises from the additional rotational degrees of freedom and does not exist for the disk or sphere packing.

There have been conjectures (*25*, *26*) that frictionless random packings have just enough constraints to completely statically define the system (*27*), $Z = 2f$ (i.e., that the system is isostatic), where f is the number of degrees of freedom per particle ($f = 3$ for spheres, $f = 5$ for spheroids, and $f = 6$ for general ellipsoids) (*28*). If friction is strong, then fewer contacts are needed, $Z = f + 1$ (*29*). Experimentally, Z for spheres was determined by Bernal and Mason by coating a system of ball bearings with paint, draining the paint, letting it dry, and counting the number of paint spots per particle when the system was disassembled (*30*). Their results gave $Z \approx 6.4$, surprisingly close to isostaticity for frictionless spheres (*31*).

We performed the same experiments with the M&M's, counting the number of true contacts between the particles (*32*). A histogram of the number of touching neighbors per particle for the regular candies is shown in Fig. 4. The average number is $Z = 9.82$. In simulations a contact is typically defined by a cutoff on the gap between the particles. Fortunately, over a wide range (10^{-9} to 10^{-4}) of contact tolerances, Z is reasonably constant. Superposed in Fig. 4 is the histogram of contact numbers obtained for simulated packings of oblate ellipsoids for $\alpha = 0.526$, from which we found $Z \approx 9.80$. In Fig. 2B we show Z as a function of aspect ratio α (*33*). As with the volume fraction, the contact number appears singular at the sphere value and rises sharply for small deviations. Unlike φ, however, Z does not decrease for large aspect ratios, but rather appears to remain constant.

We expect that fully aspherical ellipsoids, which have $f = 6$, will require even more contacts for jamming ($Z = 12$ according to the isostatic conjecture) and larger φ. Results from simulations of ellipsoids with axes $a = \alpha^{-1}$, $b = 1$, and $c = \alpha$ (where α measures the asphericity) are included in Fig. 2A. At $\alpha \approx 1.3$ we obtain a surprisingly high density of $\varphi \approx 0.735$, with no significant orientational ordering. The maximum contact number observed in Fig. 2B is $Z \approx 11.4$. It is interesting that for both spheroids and general ellipsoids, Z reaches a constant value at approximately the aspect ratio for which the density has a maximum. This supports the claim that the decrease in density for large α is due to exclusion volume effects.

The putative nonanalytic behavior of Z and φ at $\alpha = 1$ is striking and is evidently related to the randomness of the jammed state. Crystal close packings of spheres and ellipsoids show no such singular behavior, and in fact φ and Z are independent of α for small deviations from unity. On the other hand, for random packings,

the behavior is not discontinuous, whereas the number of degrees of freedom jumps from three to five (or six) as soon as α deviates from 1. In several industrial processes such as sintering and ceramic formation, interest exists in increasing the density and number of contacts of powder particles to be fused. If ellipsoidal instead of spherical particles are used, we may increase the density of a randomly poured and compacted powder to a value approaching that of the densest (fcc) lattice packing.

References and Notes

1. P. M. Chaikin, in *Soft and Fragile Matter, Nonequilibrium Dynamics, Metastability and Flow,* M. E. Cates, M. R. Evans, Eds. (Institute of Physics, London, 2000), pp. 315–348.
2. T. Aste, D. Weaire, *The Pursuit of Perfect Packing* (IOP, London, 2000).
3. J. H. Conway, N. J. A. Sloane, *Sphere Packings, Lattices, and Groups* (Springer-Verlag, New York, ed. 3, 1999).
4. A. J. Liu, S. R. Nagel, *Nature* **396**, 21 (1998).
5. H. A. Makse, J. Kurchan, *Nature* **415**, 614 (2002).
6. S. F. Edwards, in *Granular Matter,* A. Mehta, Ed. (Springer-Verlag, New York, 1994), pp. 121–140.
7. R. Zallen, *The Physics of Amorphous Solids* (Wiley, New York, 1983).
8. G. D. Scott, D. M. Kilgour, *J. Phys. D* **2**, 863 (1969).
9. S. Torquato, T. M. Truskett, P. G. Debenedetti, *Phys. Rev. Lett.* **84**, 2064 (2000).
10. A. R. Kansal, S. Torquato, F. H. Stillinger, *Phys. Rev. E* **66**, 041109 (2002).
11. The highest density is realized only by stacking variants of the fcc and hcp lattices (*34*). This is also a trivial lower bound for the maximal density of ellipsoid packings for any aspect ratio; however, it is known that higher densities are possible for sufficiently aspherical ellipsoids (*35*).
12. M&M's Candies are a registered trademark of Mars Inc.
13. We estimate the correction due to the lower density at the surface of the flasks to be about 0.005.
14. M. P. Allen, G. T. Evans, D. Frenkel, B. M. Mulder, *Adv. Chem. Phys.* **86**, 1 (1993).
15. B. D. Lubachevsky, F. H. Stillinger, *J. Stat. Phys.* **60**, 561 (1990).
16. B. D. Lubachevsky, F. H. Stillinger, E. N. Pinson, *J. Stat. Phys.* **64**, 501 (1991).
17. A. Donev, S. Torquato, F. H. Stillinger, in preparation.
18. D. Frenkel, J. F. Maguire, *Mol. Phys.* **49**, 503 (1983).
19. A. Donev, S. Torquato, F. H. Stillinger, R. Connelly, *J. Comp. Phys.*, in press.
20. S. Torquato, F. H. Stillinger, *J. Phys. Chem. B* **105**, 11849 (2001).
21. J. D. Sherwood, *J. Phys. A* **30**, L839 (1997).
22. B. J. Buchalter, R. M. Bradley, *Phys. Rev. A* **46**, 3046 (1992).
23. S. R. Williams, A. P. Philipse, *Phys. Rev. E* **67**, 051301 (2003).
24. C. R. A. Abreu, F. W. Tavares, M. Castier, *Powder Technol.* **134**, 167 (2003).
25. S. Alexander, *Phys. Rep.* **296**, 65 (1998).
26. S. F. Edwards, D. V. Grinev, *Phys. Rev. Lett.* **82**, 5397 (1999).
27. The total number of degrees of freedom would be equal to the number of impenetrability constraints (to within a constant of order 1), each of which is determined by a contact between two touching particles.
28. It is also often claimed that this is the minimal number of contacts needed to ensure jamming (*25*). However, this claim is based on a counting argument that is directly applicable only to spheres, whereas handling the impenetrability constraints for ellipsoids requires including higher order corrections because of curvature effects.
29. G. C. Barker, A. Mehta, *Phys. Rev. A* **45**, 3435 (1992).
30. J. D. Bernal, J. Mason, *Nature* **385**, 910 (1990).
31. More recent simulations and experiments give $Z \leq 6$.
32. Near neighbors (even when very close) leave a spot; touching neighbors leave a spot with a hole in the middle at the contact point.
33. Note that computer-generated packings can have a small percentage of "rattlers" (particles without any contacts that are not observable in our experiments), which we do not exclude when calculating Z.
34. T. C. Hales, xxx.lanl.gov/math.MG/9811071 (1998).
35. A. Bezdek, W. Kuperberg, in *Applied Geometry and Discrete Mathematics,* P. Gritzmann, B. Sturmfels, Eds., vol. 4 of *DIMACS Series in Discrete Mathematics and Theoretical Computer Science* (American Mathematical Society, Providence, RI, 1991), pp. 71–80.
36. J. B. Knight, C. G. Fandrich, C. N. Lau, H. M. Jaeger, S. R. Nagel, *Phys. Rev. E* **51**, 3957 (1995).
37. D. Coelho, J.-F. Thovert, P. M. Adler, *Phys. Rev. E* **55**, 1959 (1997).
38. Wall effects yield lower measured densities. Continued "tapping" of the candies may further densify the system, as happens for granular material (*36*). Furthermore, the somewhat higher density of the computer-generated packings can be explained by taking into account the influence of gravity and friction, which are not included in the simulation. Gravitation-dominated packings always have much lower packing fractions, as low as $\varphi \approx 0.4$, and have significant orientational ordering (*22, 37*).

39. Supported by American Chemical Society PRF grant 36967-AC9 (S.T., A.D., F.H.S.), NASA grant NAG3-1762 (P.M.C.), and NSF grants DMR-0213706 (S.T., P.M.C., A.D., F.H.S.), DMS-0312067 (S.T., A.D., F.H.S.), and DMS-0209595 (R.C.).

27 October 2003; accepted 9 December 2003

Renewable Hydrogen from Ethanol by Autothermal Reforming

G. A. Deluga,[1] J. R. Salge,[1] L. D. Schmidt,[1]* X. E. Verykios[2]

Ethanol and ethanol-water mixtures were converted directly into H_2 with ~100% selectivity and >95% conversion by catalytic partial oxidation, with a residence time on rhodium-ceria catalysts of <10 milliseconds. Rapid vaporization and mixing with air with an automotive fuel injector were performed at temperatures sufficiently low and times sufficiently fast that homogeneous reactions producing carbon, acetaldehyde, ethylene, and total combustion products can be minimized. This process has great potential for low-cost H_2 generation in fuel cells for small portable applications where liquid fuel storage is essential and where systems must be small, simple, and robust.

In order for hydrogen fuel cells to have a large impact on reducing greenhouse gas emissions, the hydrogen needs to be derived from sunlight, either directly or indirectly from biomass through photosynthesis. The use of hydrogen fuel cells in vehicles or in portable power plants will require lightweight H_2 storage or "on-board" reforming of hydrogen-containing compounds into H_2 (*1*).

Biomass candidates for H_2 generation include sugar, starch, oils, and crop wastes. The production of hydrogen from sugar by catalytic reaction has been demonstrated (*1*, *2*), but the process from glucose thus far has shown only 50% selectivity to H_2 and requires a long reaction time. A fuel cell operating directly on sugars has been demonstrated (*3*), but the power densities are extremely low. Biodiesel (the methyl ester of vegetable oil) should be a good candidate for direct reforming to H_2 because the analogous fossil diesel can be reformed (*4*, *5*), although the higher cost of soy oil limits its economics. Ethanol is now formed by fermentation of starch or sugar, and research suggests that it may also be produced from lower-cost vegetation such as crop wastes (*6*).

Ethanol is readily and increasingly available in the United States because of the requirement for an ethanol additive in gasoline fuels, and 2.8 billion gallons/year are now produced throughout the country by the fermentation of biomass at a cost of approximately $1 per gallon, which is competitive with petroleum fuels. However, a significant fraction of ethanol's production cost as a gasoline fuel additive comes from the need to remove all water, which requires distillation and water separation from the azeotrope using zeolite adsorption.

We recently demonstrated direct H_2 generation (*7–9*) from ethanol via oxidation, which was carried out by preheating ethanol to ~500°C over lanthanates, Ru, and Ni. There has been discussion of the desirability of autothermal reforming of ethanol (*10*), but ethanol oxidation presents energetic and flammability issues. The partial oxidation reaction

$$C_2H_5OH + \tfrac{1}{2}O_2 \rightarrow 2CO + 3H_2$$

$$\Delta H_R \cong +20 \text{ kJ/mol} \qquad (1)$$

(where ΔH_R is the enthalpy change or heat of reaction) is slightly endothermic, so this re-

[1]Department of Chemical Engineering and Materials Science, University of Minnesota, Minneapolis MN 55455, USA. [2]Department of Chemical Engineering, University of Patras, GR-26500 Patras Greece.

*To whom correspondence should be addressed. E-mail: schmidt@cems.umn.edu